Regenerative terahertz quantum detectors

Author(s):
Micheletti, Paolo; Faist, Jérôme; Olariu, Tudor; Senica, Urban; Beck, Mattias; Scalari, Giacomo

Publication date:
2021-10

Permanent link:
https://doi.org/10.3929/ethz-b-000510542

Originally published in:
APL Photonics 6(10), https://doi.org/10.1063/5.0063141

Funding acknowledgement:
724344 - On Chip Terahertz Frequency Combs (EC)

APL Photonics | ARTICLE | scitation.org/journal/app

Regenerative terahertz quantum detectors

Cite as: APL Photon. 6, 106102 (2021); doi: 10.1063/5.0063141
Submitted: 12 July 2021 • Accepted: 4 October 2021 •
Published Online: 18 October 2021

Paolo Micheletti, Jérôme Faist,[a)] Tudor Olariu, Urban Senica, Mattias Beck, and Giacomo Scalari

AFFILIATIONS

Institute for Quantum Electronics, ETH Zurich, 8093 Zürich, Switzerland

[a)] **Author to whom correspondence should be addressed:** jfaist@ethz.ch

ABSTRACT

Because of the ultrafast and photon-driven nature of the transport in their active region, we demonstrate that quantum cascade lasers can be operated as resonantly amplified terahertz detectors with wide RF bandwidth. Tunable responsivities up to 50 V/W and noise equivalent powers down to 100 pW/Hz$^{1/2}$ are demonstrated at 4.7 THz. Constant peak responsivities with respect to the detector temperature are observed up to 80 K. Thanks to the ≈ps intersub-band lifetime, electrical bandwidths larger than 20 GHz can be obtained, allowing the detection of optical beatnotes from quantum cascade THz frequency combs.

I. INTRODUCTION

Recent years saw an impressive development in the field of high speed/high frequency devices operating at THz wavelengths. Specifically, the demonstration and development of quantum cascade laser frequency combs first in the mid-IR[1] and then in the THz[2] are having a major impact in the field of spectroscopy[3] and hold high promise also for other areas such as telecom for the next 6G and local area networks.[4] As the development of THz QCL comb sources[5–7] and their understanding[8,9] proceed at a fast pace, the call for ultrafast THz detectors with high responsivity is imperative. Recent advances using graphene[10] and Quantum Well Infrared Photodetectors (QWIPs) inserted in nanoresonators[11] are promising, but a highly responsive, ultrafast, high temperature, broadband THz detector is still lacking. We propose here an implementation of the concept of regenerative amplification for the detection of THz radiation. We leverage on the ultrafast dynamics of the quantum cascade active medium driven to perform resonant detection. In a regenerative amplifier, a very large overall signal gain is achieved by positive feedback onto the input of the amplifier. Initially developed and used in early radios,[12,13] this approach was also considered for optical systems since a laser below threshold can be seen as a regenerative amplifier.[14] Low-light signal detection using regenerative amplification was investigated experimentally.[15,16] The key disadvantage of regenerative amplification is its narrow bandwidth, which is the reason why it is employed in optical systems mostly for amplification of short pulses[17] and not for the detection of optical signals. Indeed, in the visible and near infrared, photodiodes combining very large quantum efficiencies ($\eta > 0.5$) and low dark currents, combined with low noise electronics, enable extremely sensitive optical receivers to be realized.

In contrast, in the THz spectral region, this approach is much less attractive since the photon energy is smaller than $k_B T$ at room temperature. Indeed, quantum cascade detectors[18] and quantum well infrared photoconductors[19] operating in the THz have been reported, with high frequency capabilities.[20] Nevertheless, and in contrast to the situation in the mid-infrared where the use of optimal doping[21] combined with microcavities[22] enabled the operation up to room temperature, the THz QCDs[11] operate below liquid nitrogen temperatures, and excellent performances are typically obtained at 4 K. The situation is even more extreme in superconductor hot electron bolometers where very low NEPs are achieved at millikelvin temperatures.[23]

Quantum cascade lasers based on intersub-band transition have enabled the generation of coherent radiation in the mid-infrared and the development of sensing applications because of their capability to operate at room temperature. The recent improvement of terahertz quantum cascade lasers, based on the simultaneous use of larger band discontinuities combined with a simple two-well quantum cascade structure and numerical optimization, has brought the operation temperature of these devices in the range of thermoelectric (Peltier) coolers.[24–27]

One unique property of quantum cascade lasers is their ultrafast photon-driven transport, arising naturally from the combination of tunneling electron injection and an ultrashort upper state lifetime. As a result, the voltage–current characteristic of the device shows a sharp conductance discontinuity at threshold as the photon-driven transport is added to the non-radiative current.[29] The ultrafast nature of the response to that current is responsible for the very strong beatnote appearing at the round trip frequency observed in quantum cascade laser frequency combs; in this situation, the laser is detecting its own light intensity modulation.[30] Similarly, the emission of a QCL above threshold can be fed into the cavity in self-mixing schemes,[31] to achieve THz detection,[32,33] and heterodyne measurements.[34] However, the high field intensity inside the cavity prevents a QCL above threshold to detect external sources directly, i.e., without relying on the non-linear mixing between the external and internal coherent fields. Nevertheless, in the exact same way as a device can be detecting its own radiation above threshold, we anticipate that a photocurrent can be induced in a quantum cascade laser driven *below* threshold such that the active region has a positive gain. An external photon can indeed enhance the photon-driven transport, generating a photocurrent while being amplified at the same time. Therefore, in contrast to previously reported QCLs working as detectors in the mid-IR,[35] the operation as a detector relies on stimulated emission rather than photon absorption as in a standard QCD. Nevertheless, our approach holds the same potential for integration of laser and detector on the same chip.[36]

If we consider a Fabry–Pérot laser containing N_p periods and with a gain of g at the photon energy $h\nu$, the photocurrent generated in a section δz (δI_{ph}) is equal to

$$\delta I_{ph} = \frac{P_{circ}(z)}{N_p}\frac{e}{h\nu}g\delta z, \tag{1}$$

where $P_{circ}(z) = |E_{circ}(z)|^2$ is the circulating power inside the cavity. The total photocurrent can be computed by taking explicitly the spatial dependence of the field inside the laser cavity, which can be expressed as a function of net gain $g_{net} = g - \alpha_w$ (where g is the gain and α_w represents the waveguide losses) and amplitude mirror reflectivities r_1 and r_2 for every wavelength λ,[14]

$$E_{circ}(z) = \frac{E_{in}\sqrt{\eta_{opt}(1-|r_1|^2)}}{1 - r_1 r_2 e^{(g_{net}-2ik)L_{cav}}} \times \left[e^{-(g_{net}/2+ik)z} + r_2 e^{(g_{net}/2+ik)z}\right], \tag{2}$$

where E_{in} is the incoming optical field and $k = 2\pi/\lambda$. An optical efficiency η_{opt} is introduced to take into account the fraction of incoming power effectively coupled into the laser cavity. Integrating δI over the whole cavity length L_{cav} yields the total photocurrent,

$$I_{ph} = \frac{P_{circ}(0)}{h\nu/q_0 N_p}\frac{g}{\alpha_w - g}\left[e^{-g_{net}L_{cav}} - 1 + |r_2|^2\left(1 - e^{g_{net}L_{cav}}\right)\right]. \tag{3}$$

The resonant nature of the photocurrent derives directly from Eq. (2), which fixes a relation between the optical gain and detection bandwidth Δf for every mode of the cavity,

$$\Delta f = \frac{c}{2\pi n L_{cav}} arcos\left(2 - \frac{1 + e^{2(g_{net}-\alpha_m)L_{cav}}}{2e^{(g_{net}-\alpha_m)L_{cav}}}\right), \tag{4}$$

where n is the refractive index inside the cavity. Δf tends to vanish as the gain approaches the theoretical limit α_m at which the photocurrent diverges. However, the device stability and the noise prevent this limit to be reached in real applications. When considering a microcavity device, the spatial dependence of the field can then be neglected. Thus, it is more convenient to consider the photocurrent generated in the time interval dt and integrate it on the photon lifetime in the cavity (SM1 of the supplementary material). Expressing the gain γ, the waveguide losses Γ_Ω, and the radiative losses Γ_{rad} as rates [Fig. 1(a)] allows us to write the responsivity $\mathscr{R}$ (in A/W) on resonance as

$$\mathscr{R} = \frac{1}{N_p}\frac{e}{h\nu}\frac{4\gamma\Gamma_{rad}}{(\Gamma_{rad} + \Gamma_\Omega - \gamma)^2}, \tag{5}$$

where the gain γ, the waveguide losses Γ_Ω, and the radiative losses Γ_{rad} are now expressed as rates [Fig. 1(a)]. In contrast to conventional photodetectors, the dark current i_d required to maintain the gain is relatively large such that the dynamical impedance of the device must be taken into account to evaluate the voltage responsivity. The dynamical impedance can be estimated in an analytical model by using the density matrix approach first developed by Kazarinov and Suris[37] in the case of a superlattice and then extended to quantum cascade lasers.[29] In this way, the current density J flowing between the injector sub-band and the upper state detuned in energy by an amount $\hbar\Delta$ is proportional to their population difference Δn,

$$J(\Delta, \Delta n) = \frac{2e|\Omega_{3i}|^2}{\tau_\parallel}\frac{\Delta n}{\Delta^2 + 1/\tau_\parallel^2}, \tag{6}$$

where $\tau_\parallel$ is the in-plane scattering lifetime and $\hbar\Omega_{3i}$ is the coupling between the sub-bands. When combined with a rate equation for the upper state and assuming a constant total electron density between the two sub-bands, expression (6) yields for the current density for a given radiative current J_{rad} from the upper state,

$$J(\Delta, J_{rad}) = \frac{2e|\Omega_{3i}|^2\tau_\parallel}{1 + \Delta^2\tau_\parallel^2 + 4\Omega_{3i}^2\tau_3\tau_\parallel}\left(n_s + \frac{2\tau_3}{e}J_{rad}\right), \tag{7}$$

where τ_3 is the upper state population lifetime. Equation (7) reverts back to the well-known result at $J_{rad} = 0$. Using the above result, the differential photoresistance (per period) can be extracted by computing

$$R_d = \frac{\hbar}{e}\frac{\partial\Delta}{\partial J_{rad}}\bigg|_{dJ=0} = \frac{\hbar}{e^2\Delta n_s}\frac{\tau_3}{\tau_\parallel^2}\left(\Delta^2\tau_\parallel^2 + 1 + 4|\Omega_{3i}|^2\tau_3\tau_\parallel\right). \tag{8}$$

This resistance is, in general, smaller than the differential resistance of the structure operated below threshold,

$$R_{\rm nr} = \frac{\hbar}{e}\frac{\partial\Delta}{\partial J}\bigg|_{J_{rad}=0} = -\frac{\hbar}{e^2\Delta n_s}\frac{\left(\Delta^2\tau_\parallel^2 + 1 + 4|\Omega_{3i}|^2\tau_3\tau_\parallel\right)^2}{4|\Omega_{3i}|^2\tau_\parallel^3}. \tag{9}$$

Indeed, the ratio of these two resistances is given by

$$\frac{R_d}{R_{\rm nr}} = -\frac{4|\Omega_{3i}|^2\tau_\parallel\tau_3}{\Delta^2\tau_\parallel^2 + 1 + 4|\Omega_{3i}|^2\tau_\parallel\tau_3}. \tag{10}$$

As the photovoltage is proportional to R_d and the noise voltage (caused by shot noise) is proportional to $R_{\rm nr}$, it is, of course,

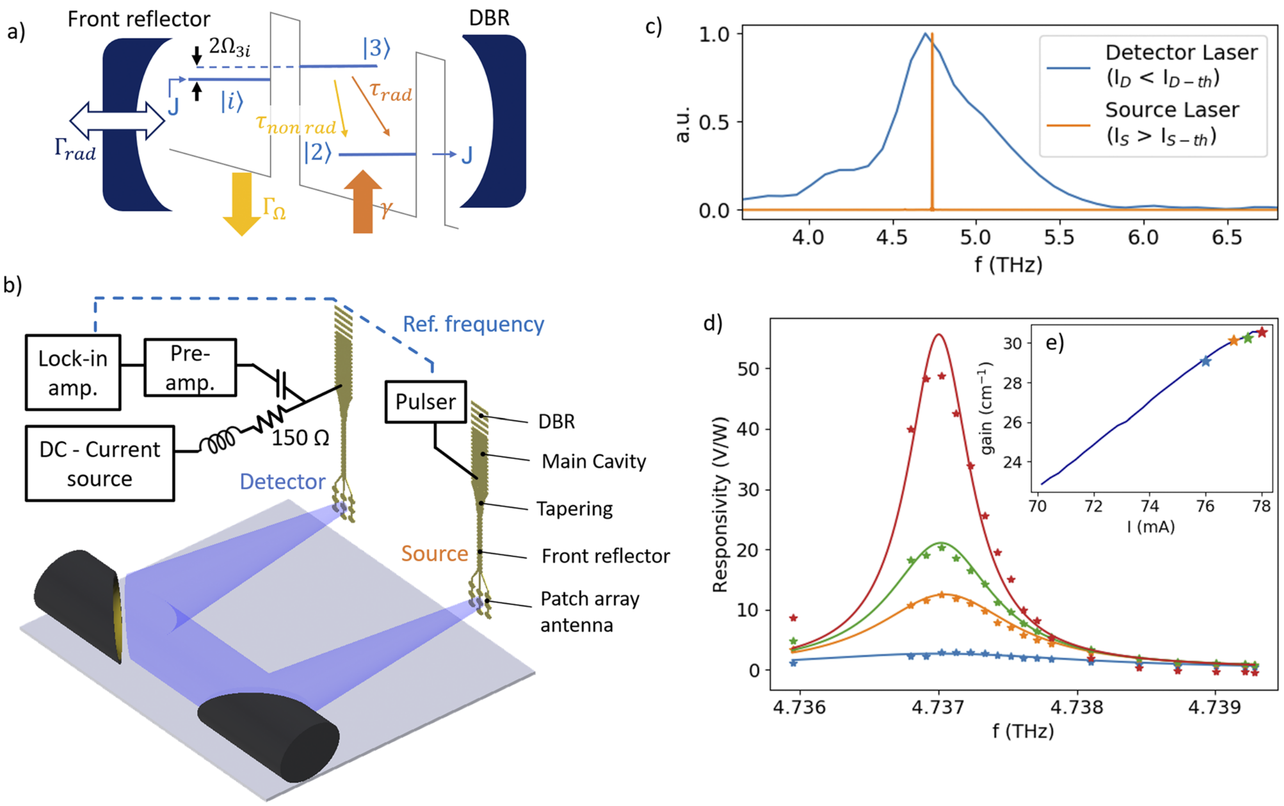

FIG. 1. Regenerative Terahertz Quantum Detector (ReTeD). (a) Schematic representation of the resonant cavity with the relevant parameters entering equation for the responsivity (5). (b) Experimental setup: The source laser is driven in the pulsed mode and its emission focused onto the detector laser driven in the continuous wave below threshold. The signal is detected on a 150 Ω load resistor placed in series with the laser. The different parts composing the patch-array antenna-single-mode QCL are indicated. (c) Spectra of the luminescence of the detector laser below threshold (blue) and of the emission source laser above threshold (orange). (d) Detector responsivity as a function of source frequency for different detector bias currents. The source laser frequency was characterized with a Bruker Vertex 80 FTIR using zero padding to get a more accurate peak position.[28] For each current, the experimental data are fitted with Eq. (3). The values of gain resulting from the fit are reported in (e) as a function of detector bias current. The points corresponding to the curves reported in (d) are indicated by the colored ⋆.

desirable to bring the above ratio as close to unity as possible. This is the case for thin injection barriers in the strong coupling limit defined by

$$4|\Omega_{3i}|^2\tau_{\parallel}\tau_3 \gg 1. \tag{11}$$

This result enables us to write the noise equivalent power of the device, assuming that the noise is dominated by the shot noise,

$$\mathrm{NEP} = \frac{\sqrt{2ei_dB}}{\mathscr{R}}\frac{R_{\mathrm{nr}}}{R_d}, \tag{12}$$

where i_d is the current and the noise is detected in a bandwidth B.

II. EXPERIMENTAL RESULTS

An implementation of the Regenerative Terahertz Quantum Detector (ReTeD) is achieved exploiting a patch-array antenna-single-mode QCL[38] [Fig. 1(b)]. The device consists of a double metal waveguide with a distributed Bragg reflector (DBR) acting as a high reflectivity mirror and a first order distributed feedback (DFB) grating acting as a narrow-band front mirror. The two mirrors are designed with the help of finite element simulations performed with COMSOL, which yielded a back mirror reflectivity of $R_{back} = 0.95$[39] and a front mirror reflectivity of $R_{front} = 0.85$ with a bandwidth of ≈ 100 GHz (SM2 of the supplementary material). A patch-array antenna, integrated with the top metal contact, provides for efficient light out-coupling. At the same time, it eases the in-coupling of light into the double metal waveguide, thus making the device suitable to work as both laser and ReTeD. An in-coupling efficiency of 18% is estimated with a full-wave 3D numerical simulation performed with the software CST (SM2 of the supplementary material). None of the optical elements of the device is expected to limit the detection bandwidth of the main mode, which is rather fixed by the gain-bandwidth relation [Eq. (4)]. However, the front mirror bandwidth does reduce the gain available for the other cavity modes, thus limiting the overall detection bandwidth.

Two devices processed from the same wafer are used in the experiment, and the emission of one laser, used as source, is focused onto the second, which is kept *below threshold* and is used as a detector [see the experimental layout in Fig. 1(b)]. The spectra of the two lasers are centered around the same frequency (4.737 THz), as shown in Fig. 1(c), where the luminescence of the detector laser is compared with the spectrum of the source laser above threshold. The optical resonant response of the detector is measured by temperature tuning the source laser in the range of 10–55 K for fixed values of the detector laser current. As the detector bias is increased but maintained below threshold, the gain of the structure grows, resulting in a higher responsivity and a narrower optical bandwidth. For current values above threshold, the radiation emitted by the active region of the detector rapidly overcomes the incoming one. As shown in Fig. 1(d) where the experimental responsivity is reported as a function of optical frequency, the resonant nature of the detector is clearly apparent. Increasing the detector bias current toward threshold leads to responsivities up to 50 V/W, while the detection bandwidths decrease. This resonant behavior can be described with good accuracy by our model where $\mathscr{R}_{V/W} = I_{ph}R_d/P_{in}$ and I_{ph} is computed from Eq. (3), assuming values of parameters described in detail in SM2 of the supplementary material. In particular, the values of optical gain assumed to compute the responsivities as a function of bias current are shown in Fig. 1(e). The optical efficiency η_{opt} = 12% is deduced from a comparison of the slope efficiency of the laser with the theoretical value. For each value of the injected current, the fit also yields a value of the differential photoresistance in the range of R_d = 2–5 Ω. This value is reported in Fig. 2 and can be compared to the expected one derived from the Kazarinov–Suris model of transport (8). First, a Schrödinger–Poisson self-consistent solver is used to convert the applied bias into a detuning Δ. The computed coupling between the injector and the upper state

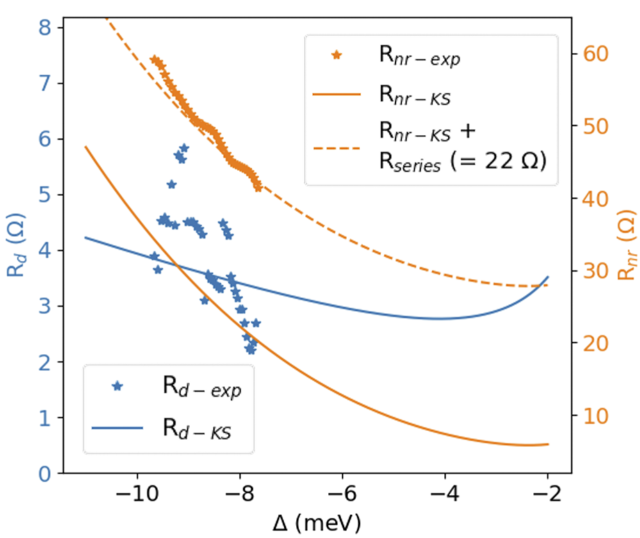

FIG. 2. Non-radiative differential resistance (R_{NR}) and photoresistance (R_d) as a function of energy detuning Δ. The orange ⋆ represents the experimental non-radiative resistances ($R_{nr\text{-exp}}$) measured in CW at a temperature of 20 K. The non-radiative resistance calculation based on the Kazarinov–Suris model [Eq. (9)] is depicted with the orange solid line, and the dashed line represents the same quantity with the addition of the series resistance (R_{series} = 22 Ω). The photoresistance is reported in blue. ⋆ indicates the values resulting from the fitting of the experimental measurement of responsivity with Eq. (3) ($R_{d\text{-exp}}$), while the solid line indicates the calculation based on the Kazarinov–Suris model $R_{d\text{-}KS}$ [Eq. (8)].

wavefunction $\hbar\Omega_{3i}$ = 0.8 meV was adjusted down to $\hbar\Omega_{3i}$ = 0.45 meV to obtain a better fit to the data. We also obtained the electronic lifetimes $\tau_\parallel$ = 0.31 ps and τ_2 = 4.7 ps from a measurement of the device electroluminescence linewidth [Fig. 1(c)] and maximum current density, respectively. As shown in Fig. 2, while the experimental differential resistance of the device R_{nr} agrees well with the computed one [assuming an additional series resistance of 22 Ω (SM3 of the supplementary material)], the observed differential resistance R_d shows a much stronger field dependence than predicted in our simple model, probably reflecting the well-known limitations of this simplified approach. This analysis, however, points toward the relatively low ratio $R_d/R_{NR} \approx 8\%$ as strongly limiting the device's performance. Increasing this value could be achieved, for instance, by using thinner injector-upper state barriers to obtain a stronger injection $4|\Omega_{3i}|^2\tau_\parallel\tau_3$ above the value of 3 used in this device.

The noise of the detector is evaluated connecting a spectrum analyzer to the detector under bias while keeping the source laser off. From the measurement of the noise, the minimum NEP is calculated using the responsivity obtained in the resonant case [Fig. 3(a)], i.e., when the source and detector laser frequencies match. Values smaller than 100 pW/Hz$^{1/2}$ can be reached close to threshold. A good agreement is obtained with the theoretical NEP computed considering only the bias current shot noise, showing the shot noise to be effectively the dominant source of noise of the detector. As the signal is proportional to R_d and the noise is proportional to R_{NR}, an improvement of this ratio would also benefit the NEP. A key feature of this approach to detect THz radiation is that the peak responsivity does not depend on the detector's temperature as long as it is below the maximum operating temperature of the laser. The decrease in upper state lifetime due to temperature increase indeed only shifts the threshold to higher values, resulting in a slightly larger noise level. As a result, the detector performances are expected to show only a weak temperature dependence.

The detector's temperature dependence is investigated experimentally and shown in Fig. 3(b). In this measurement, a detector laser with a slightly higher central frequency is used such that the frequency matching between the source and detector QCL is obtained when the temperature of the source is smaller than the one of the detector. The result shows that the peak responsivity stays approximately constant until 80 K ($T_{D\text{-max}}$), temperature at which the detector cannot reach its threshold anymore (SM4 of the supplementary material). Below $T_{D\text{-max}}$, the peak responsivity lies in the 20–25 V/W range. This value is comparable with the one obtained with the detector laser used in the previous experiment. Above the maximum operating temperature, the maximum gain of the active region starts to decrease, resulting in a reduced peak responsivity. The NEP relative to each point is computed from the bias current shot noise. Despite the fact that at higher temperatures the maximum responsivity is obtained at higher currents, due to the increase in threshold current, the NEP does not increase dramatically, thanks to the decrease in non-radiative resistance with temperature. Above $T_{D\text{-max}}$, the decrease in gain, hence of responsivity, causes a substantial increase in NEP.

Another fundamental advantage of exploiting QCLs for THz radiation detection is that, thanks to the ultrafast nature of the photon-driven transport in a QCL, the response of the ReTeD can be extremely fast. The fact that electrical beatnotes of the order of

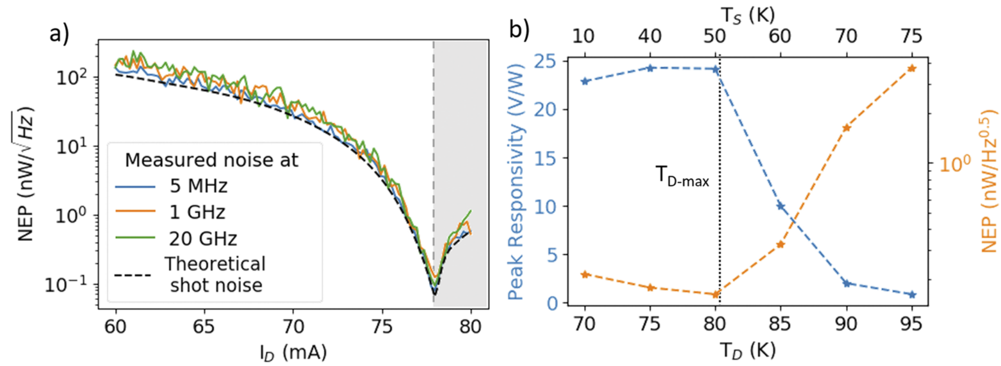

FIG. 3. NEP as a function of detector bias current (a). The NEP computed as $NEP = N/\mathscr{R}_{V/W}/R_{NR}$ is reported in the solid lines. The power noise N is measured with a Rohde and Schwarz FSW-67 spectrum analyzer connected to the detector load resistor. Noise spectra from DC to 25 GHz are measured for different detector biases with a resolution bandwidth of 10 Hz and averaging over ten samples. The results reported in the plot are relative to frequencies of 5 MHz (blue), 1 GHz (orange), and 20 GHz (green) and a device temperature of 15 K. The NEP obtained considering only the detector bias current shot noise ($N = 2eI_dBR_{NR}$) is depicted with the dashed line. The gray area represents the region above threshold. Peak responsivity as a function of detector laser temperature (b). The source laser is driven in the pulsed mode with a fixed peak current (209 mA). For each temperature of the detector, the source laser temperature is tuned to maximize the optical signal. The maximum responsivity reached by sweeping the detector bias is reported in blue. The NEP corresponding each responsivity and calculated from the bias current shot noise is reported in orange. The dashed line indicates the temperature at which the detector laser cannot reach threshold.

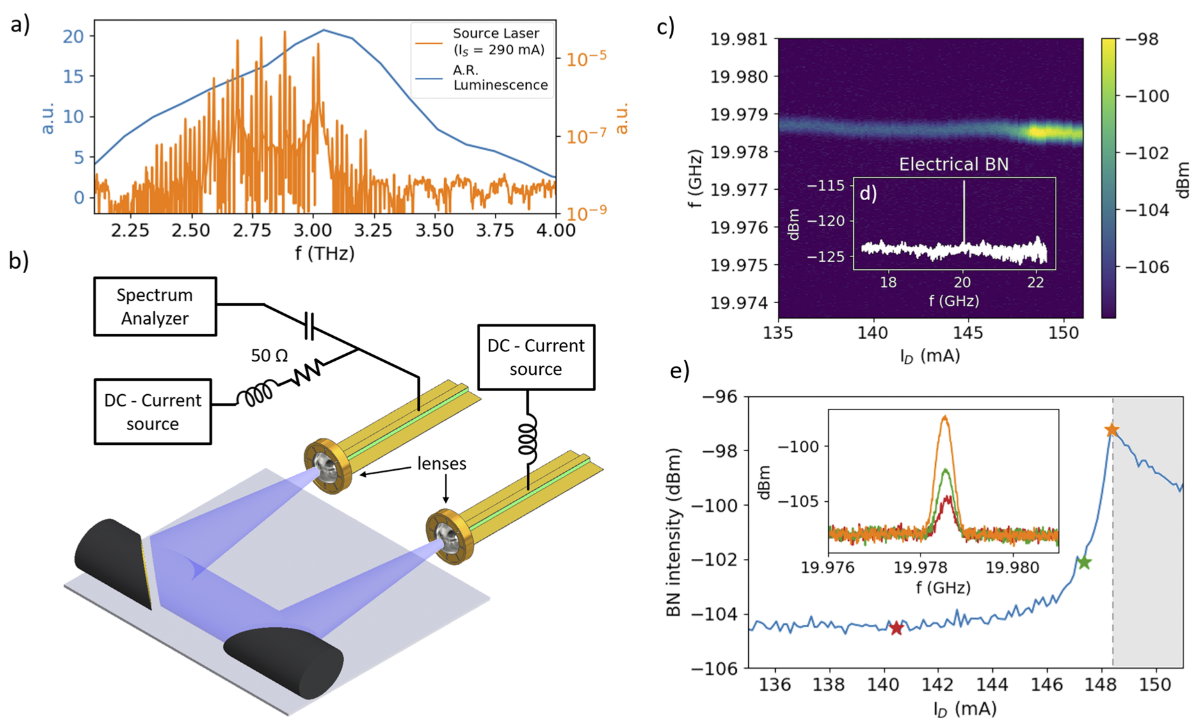

FIG. 4. Optical detection of the beatnote at GHz frequencies. (a) Comparison between the Active Region (AR) electroluminescence and spectrum of the source laser. The AR luminescence (blue trace) is measured on a 0.345 mm long and 70 μm wide non-lasing device biased at 8 V and kept at 10 K.[6] The source laser spectrum (orange trace) is measured with a Bruker Vertex 80 FTIR. The laser is kept at 15 K and driven CW at I_S = 290 mA. Schematic of the experimental setup (b). The source and detector laser are placed on the foci of the parabolic mirrors. Both lasers are driven in CW, and a 50 Ω load resistor is placed in series with the current source of the detector laser. A Rohde and Schwarz FSW-67 spectrum analyzer is also connected to the detector QCL through a bias-tee. Optical beatnote map as a function of detector bias current (c). The source laser bias is fixed at 290 mA and kept at 15 K. The detector laser temperature is 25 K, and its bias is swept from 135 to 151 mA. The spectrum analyzer is operated with a resolution bandwidth of 10 kHz. For each current, the measurement is averaged over 20 samples. The electrical beatnote measured on the bias-tee of the source laser is reported in the inset. Maximum value of the beatnote intensity as a function of detector current (e). The gray area indicates the region above threshold, which is, in this configuration, $I_{D\text{-}th}$ = 148.4 mA. The colored ⋆ refers to the BN spectra reported in the inset.

several tens of GHz can be observed in THz QCL frequency combs[2,6,40–41] suggests indeed that the cutoff frequency of the ReTeD response should lie in the same range. The easiest way to verify this hypothesis is to optically measure the beatnote of a THz frequency comb employing the ReTeD. The device presented so far is strictly single mode above threshold; therefore, it is not suitable for this purpose. For this reason, a pair of lasers based on a broadband active region[6] is used, whose emission is centered around 3 THz [Fig. 4(a), blue trace]. The devices consist of a double metal waveguide ridge of 2 mm long and 40 μm wide. A silicon lens is placed on the front facet in order to lower its reflectivity and optimize the coupling inside/outside of the ridge. The source laser is placed in one of the foci of the setup and biased in CW at I_S = 290 mA. At this current, the laser is in a comb state, displaying a wide spectrum with a bandwidth of ≈900 GHz and a single electrical beatnote at ≈20 GHz [Fig. 4(a)] orange trace (d). The electroluminescence of the detector [blue trace, Fig. 4(a)] overlaps very well with the laser's signal. The detector is placed in front of the other mirror, connected to a spectrum analyzer through a bias-tee, and always biased below the lasing threshold. In this configuration, a clear optical beatnote can be observed on the spectrum analyzer for different biases of the detector laser [Fig. 4(c)], thus confirming that the electrical bandwidth of the detector is as high as 20 GHz. We would like to underline that we are not detecting the heterodyne beating of the incoming laser signal with the receiver coherent field,[34] as our detector is always below threshold. The detected signal comes from the amplification of the coherent modes of the incoming comb inside the detector's cavity; their beating then modulates the detector current. The increase in gain as the detector current is brought toward the threshold is also reflected into an increase in the optical beatnote intensity [Figs. 4(c), 4(e), and 4(f)].

III. DISCUSSION AND CONCLUSION

We presented the application of the concept of regenerative amplification to THz detection exploiting QCL active regions as the gain medium. The ultrafast photon driven transport that characterizes QCLs offers the possibility of reaching high responsivities, wide electrical bandwidths, and high operating temperatures. The ultrafast resonant response makes the ReTeD particularly suited to characterize coherent sources and to be used for heterodyne detection. Nevertheless, the tunable optical bandwidth also allows us to detect broader sources such as blackbody emission. A very promising outlook on future architectures is represented by microcavity devices. Thanks to the higher resistance, a microresonator would lead to higher responsivities and lower NEP with respect to a Fabry–Pérot device. Considering a $(10 \times 10)\ \mu\text{m}^2$ LC microresonator with a quality factor of Q = 13, relative to α_m = 6 cm^{-1} and α_w = 25 cm^{-1}, responsivities up to 100 kV/W and NEP down to 1.6 pW/Hz$^{1/2}$ can be obtained at 3.9 THz, with a gain of 30 cm^{-1} and a current density of 2.5 kA/cm^{-2}.[25] Such active region characteristics correspond to the high performance two-well operating up to 210 K: In this perspective, we would obtain a highly responsive device up to high temperatures. The inherent ultrafast bandwidth of the detection mechanism would then be fully exploited in a microcavity geometry that reduces to the minimum the capacitive and inductive parasitics. Studies using lenses-coupled broadband lasers proved the possibility of recording optical beatnotes, thus confirming that bandwidths as high as 20 GHz can be reached with our approach and very likely can be extended to much higher frequencies as electrical beatnotes from THz QCLs have been detected up to 50 GHz and higher.[41] Regenerative amplification proves to be an effective method for detecting THz radiation and has the potential to overcome the existing technology.

SUPPLEMENTARY MATERIAL

See the supplementary material for details about the device simulations and additional supporting measurements.

ACKNOWLEDGEMENTS

The authors acknowledge the financial support from the Swiss National Science Foundation (SNF) and from the H2020 European Research Council Consolidator (Grant No. 724344) (CHIC).

AUTHOR DECLARATIONS

Conflict of Interest

The authors have no conflicts to disclose.

DATA AVAILABILITY

The data that support the findings of this study are available from the corresponding author upon reasonable request.

REFERENCES

[1] A. Hugi, G. Villares, S. Blaser, H. C. Liu, and J. Faist, "Mid-infrared frequency comb based on a quantum cascade laser," Nature **492**, 229–233 (2012).

[2] D. Burghoff, T.-Y. Kao, N. Han, C. W. I. Chan, X. Cai, Y. Yang, D. J. Hayton, J.-R. Gao, J. L. Reno, and Q. Hu, "Terahertz laser frequency combs," Nat. Photonics **8**, 462–467 (2014).

[3] G. Villares, A. Hugi, S. Blaser, and J. Faist, "Dual-comb spectroscopy based on quantum-cascade-laser frequency combs," Nat. Commun. **5**, 5192–5199 (2014).

[4] T. Harter, S. Muehlbrandt, S. Ummethale, A. Schmid, S. Neiien, L. Hahn, W. Freude, and C. Koos, "Silicon-plasmonic integrated circuits for terahertz signal generation and coherent detection," Nat. Photonics **12**, 625 (2018).

[5] M. Rösch, M. Beck, M. J. Süess, D. Bachmann, K. Unterrainer, J. Faist, and G. Scalari, "Heterogeneous terahertz quantum cascade lasers exceeding 1.9 THz spectral bandwidth and featuring dual comb operation," Nanophotonics **7**, 237–242 (2018).

[6] A. Forrer, M. Franckié, D. Stark, T. Olariu, M. Beck, J. Faist, and G. Scalari, "Photon-driven broadband emission and frequency comb RF injection locking in THz quantum cascade lasers," ACS Photonics **7**, 784–791 (2020).

[7] A. Di Gaspare, L. Viti, H. E. Beere, D. D. Ritchie, and M. S. Vitiello, "Homogeneous quantum cascade lasers operating as terahertz frequency combs over their entire operational regime," Nanophotonics **10**, 181–186 (2021).

[8] N. Opačak and B. Schwarz, "Theory of frequency-modulated combs in lasers with spatial hole burning, dispersion, and kerr nonlinearity," Phys. Rev. Lett. **123**, 243902 (2019).

[9] D. Burghoff, "Unraveling the origin of frequency modulated combs using active cavity mean-field theory," Optica **7**, 1781–1787 (2020).

[10] L. Viti, D. G. Purdie, A. Lombardo, A. C. Ferrari, and M. S. Vitiello, "HBN-encapsulated, graphene-based, room-temperature terahertz receivers, with high speed and low noise," Nano Lett. **20**, 3169–3177 (2020).

[11] M. Jeannin, T. Bonazzi, D. Gacemi, A. Vasanelli, S. Suffit, L. Li, A. G. Davies, E. Linfield, C. Sirtori, and Y. Todorov, "High temperature metamaterial terahertz quantum detector," Appl. Phys. Lett. **117**, 251102 (2020).

[12] E. H. Armstrong, "Some recent developments in the audion receiver," Proc. Inst. Radio Eng. **3**, 215–238 (1915).

[13]E. H. Armstrong, "Some recent developments of regenerative circuits," Proc. Inst. Radio Eng. **10**, 244–260 (1922).
[14]A. E. Siegman, *Lasers* (University Science Books, Mill Valley, CA, 1986), p. 14525287.
[15]I. Littler, S. Balle, K. Bergmann, G. Vemuri, and R. Roy, "Detection of weak signals via the decay of an unstable state: Initiation of an injection-seeded laser," Phys. Rev. A **41**, 4131–4134 (1990).
[16]I. C. M. Littler, K. Bergmann, and R. Roy, "Regenerative amplification of a weak Cw optical signal in an active frequency shifted feedback cavity," Opt Commun. **87**, 53–60 (1992).
[17]J. Squier, F. Salin, G. Mourou, and D. Harter, "100-Fs pulse generation and amplification in Ti-Al_2O_3," Opt. Lett. **16**, 324–326 (1991).
[18]M. Graf, G. Scalari, D. Hofstetter, J. Faist, H. Beere, E. Linfield, D. Ritchie, and G. Davies, "Terahertz range quantum well infrared photodetector," Appl. Phys. Lett. **84**, 475–477 (2004).
[19]H. C. Liu, C. Y. Song, A. J. SpringThorpe, and J. C. Cao, "Terahertz quantum-well photodetector," Appl. Phys. Lett. **84**, 4068–4070 (2004).
[20]H. Li, W. J. Wan, Z. Y. Tan, Z. L. Fu, H. X. Wang, T. Zhou, Z. P. Li, C. Wang, X. G. Guo, and J. C. Cao, "6.2-GHz modulated terahertz light detection using fast terahertz quantum well photodetectors," Sci. Rep. **7**, 3452–3458 (2017).
[21]M. R. Hao, Y. Yang, S. Zhang, W. Z. Shen, H. Schneider, and H. C. Liu, "Near-room-temperature photon-noise-limited quantum well infrared photodetector," Laser Photonics Rev. **8**, 297–302 (2014).
[22]D. Palaferri, Y. Todorov, A. Bigioli, A. Mottaghizadeh, D. Gacemi, A. Calabrese, A. Vasanelli, L. Li, A. G. Davies, E. H. Linfield, F. Kapsalidis, M. Beck, J. Faist, and C. Sirtori, "Room-temperature nine-μm-wavelength photodetectors and GHz-frequency heterodyne receivers," Nature **556**, 85–88 (2018).
[23]A. Shurakov, Y. Lobanov, and G. Goltsman, "Superconducting hot-electron bolometer: From the discovery of hot-electron phenomena to practical applications," Supercond. Sci. Technol. **29**, 023001 (2015).
[24]M. Franckié and J. Faist, "Bayesian optimization of terahertz quantum cascade lasers," Phys. Rev. Appl. **13**, 034025 (2020).
[25]L. Bosco, M. Franckié, G. Scalari, M. Beck, A. Wacker, and J. Faist, "Thermoelectrically cooled THz quantum cascade laser operating up to 210 K," Appl. Phys. Lett. **115**, 010601 (2019).
[26]A. Khalatpour, A. K. Paulsen, C. Deimert, Z. R. Wasilewski, and Q. Hu, "High-power portable terahertz laser systems," Nat. Photonics **15**, 16 (2020).
[27]M. A. Kainz, M. P. Semtsiv, G. Tsianos, S. Kurlov, W. T. Masselink, S. Schönhuber, H. Detz, W. Schrenk, K. Unterrainer, G. Strasser *et al.*, "Thermoelectric-cooled terahertz quantum cascade lasers," Opt. Express **27**, 20688–20693 (2019).
[28]M. Rösch, G. Scalari, M. Beck, and J. Faist, "Octave-spanning semiconductor laser," Nat. Photonics **9**, 42–47 (2015).
[29]C. Sirtori, F. Capasso, J. Faist, A. L. Hutchinson, D. L. Sivco, and A. Y. Cho, "Resonant tunneling in quantum cascade lasers," IEEE J. Quantum Electron. **34**, 1722–1729 (1998).
[30]H. Li, P. Laffaille, D. Gacemi, M. Apfel, C. Sirtori, J. Leonardon, G. Santarelli, M. Rösch, G. Scalari, M. Beck, J. Faist, W. Hänsel, R. Holzwarth, and S. Barbieri, "Dynamics of ultra-broadband terahertz quantum cascade lasers for comb operation," Opt. Express **23**, 33270–33294 (2015).
[31]S. Donati, *Electro-optical Instrumentation: Sensing and Measuring with Lasers* (Pearson Education, 2004).
[32]A. Valavanis, P. Dean, Y. L. Lim, R. Alhathlool, M. Nikolic, R. Kliese, S. P. Khanna, D. Indjin, S. J. Wilson, A. D. Rakic *et al.*, "Self-mixing interferometry with terahertz quantum cascade lasers," IEEE Sens. J. **13**, 37–43 (2012).
[33]P. Dean, Y. L. Lim, A. Valavanis, R. Kliese, M. Nikolić, S. P. Khanna, M. Lachab, D. Indjin, Z. Ikonić, P. Harrison *et al.*, "Terahertz imaging through self-mixing in a quantum cascade laser," Opt. Lett. **36**, 2587–2589 (2011).
[34]H. Li, Z. Li, W. Wan, K. Zhou, X. Liao, S. Yang, C. Wang, J. C. Cao, and H. Zeng, "Toward compact and real-time terahertz dual-comb spectroscopy employing a self-detection scheme," ACS Photonics **7**, 49–56 (2019).
[35]B. Schwarz, P. Reininger, H. Detz, T. Zederbauer, A. Maxwell Andrews, S. Kalchmair, W. Schrenk, O. Baumgartner, H. Kosina, and G. Strasser, "A bi-functional quantum cascade device for same-frequency lasing and detection," Appl. Phys. Lett. **101**, 191109 (2012).
[36]B. Schwarz, P. Reininger, D. Ristanić, H. Detz, A. M. Andrews, W. Schrenk, and G. Strasser, "Monolithically integrated mid-infrared lab-on-a-chip using plasmonics and quantum cascade structures," Nat. Commun. **5**, 4085–4087 (2014).
[37]R. Kazarinov and R. Suris, "Electric and Electromagnetic properties of semiconductors with a superlattice," Sov. Phys. Semiconduct. **6**, 120–134 (1972).
[38]L. Bosco, C. Bonzon, K. Ohtani, M. Justen, M. Beck, and J. Faist, "A patch-array antenna single-mode low electrical dissipation continuous wave terahertz quantum cascade laser," Appl. Phys. Lett. **109**, 201103 (2016).
[39]L. Bosco, "THz quantum cascade laser: Astrophysical applications and high temperature performance," Ph.D. thesis, ETH Zurich, 2020.
[40]M. Rösch, G. Scalari, G. Villares, L. Bosco, M. Beck, and J. Faist, "On-chip, self-detected terahertz dual-comb source," Appl. Phys. Lett. **108**, 171104 (2016).
[41]A. Forrer, Y. Wang, M. Beck, A. Belyanin, J. Faist, and G. Scalari, "Self-starting harmonic comb emission in THz quantum cascade lasers," Appl. Phys. Lett. **118**, 131112 (2021).